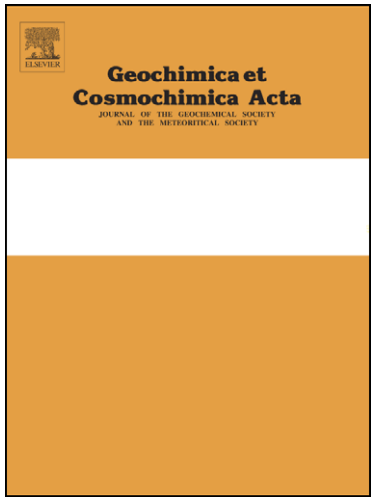

Accounting for long alpha-particle stopping distances in (U–Th–Sm)/He geochronology: 3D modeling of diffusion, zoning, implantation, and abrasion

Cécile Gautheron, Laurent Tassan-Got, Richard A. Ketcham, Katherine J. Dobson

PII: S0016-7037(12)00473-5
DOI: http://dx.doi.org/10.1016/j.gca.2012.08.016
Reference: GCA 7867

To appear in: *Geochimica et Cosmochimica Acta*

Received Date: 11 December 2011
Accepted Date: 9 August 2012

Please cite this article as: Gautheron, C., Tassan-Got, L., Ketcham, R.A., Dobson, K.J., Accounting for long alpha-particle stopping distances in (U–Th–Sm)/He geochronology: 3D modeling of diffusion, zoning, implantation, and abrasion, *Geochimica et Cosmochimica Acta* (2012), doi: http://dx.doi.org/10.1016/j.gca.2012.08.016

Accounting for long alpha-particle stopping distances in (U–Th–Sm)/He geochronology: 3D modeling of diffusion, zoning, implantation, and abrasion

Cécile Gautheron[1*], Laurent Tassan-Got[2], Richard A. Ketcham[3] and Katherine J. Dobson[4]

[1] UMR Interactions et Dynamique des Environnements de Surface – CNRS-UPS 8148, Université Paris Sud, 91405 Orsay, France, cecile.gautheron@u-psud.fr

[2] Institut de Physique Nucléaire, CNRS/IN_2P_3, Université Paris Sud, 91405 Orsay, France, tassango@ipno.in2p3.fr

[3] Jackson School of Geosciences, The University of Texas at Austin, Austin, TX, USA; ketcham@jsg.utexas.edu

[4] School of Materials, Manchester X-ray Imaging Facility, University of Manchester, M13 9PL, UK. katherine.dobson@manchester.ac.uk

* corresponding author

Abstract: In apatite (U-Th)/He thermochronology the helium distribution in a crystal is a function of the simultaneous processes of radiogenic production, thermally activated volume diffusion and the ejection of He caused by long alpha stopping distances. These processes are further complicated by zonation of U, Th and Sm within the grain and implantation of ^{4}He from neighboring U-Th-Sm bearing minerals. We use a refined version of the 3D Monte Carlo diffusion code of Gautheron and Tassan-Got (2010) to simulate the interplay between ejection and diffusion with or without zonation, ejection and abrasion for a suite of thermal histories. We examine the phenomenon of over-correction produced by the alpha ejection correction parameter (F_T or F_{ZAC} for homogeneous or heterogeneous eU repartition) by comparing the raw (measured) and F_T- or F_{ZAC}-corrected ages for a number of scenarios to the ejection-free age (A_{EF}), which we define as the age that would be obtained if alpha ejection had not occurred, or equivalently if the stopping distance was zero. We show that the use of F_T- or F_{ZAC}-corrected ages generally reproduces the ejection-free age to within typical (U-Th)/He uncertainties (± 8 %), even for zoned apatites. We then quantify the effect of alpha implantation on (U-Th)/He ages, showing that implantation from a single external source with modest relative U or Th enrichment can generate as much as 50 % excess He. For more extreme cases where an apatite is surrounded by multiple external sources the measured age can be > 300 % of that determined from an isolated crystal. While abrasion of the outer 20-25 microns can significantly reduce the age dispersion for rapidly cooled samples, slowly cooled samples can still retain 10-30 % excess He. The removal of the rim of the crystal reduces the thermal information from very low temperatures (< 40 °C), and introduces additional technical complications and biases, and should therefore be used with caution. Overall we demonstrate that although zonation and implantation may not be routinely determined, we now have the 3D modeling capability to fully investigate and constrain the causes of age

dispersion within a sample, leading to significant improvement in our ability to interpret (U-Th)/He data.

1. Introduction

The apatite (U-Th)/He (AHe) low temperature thermochronometer is frequently used to constrain exhumation and burial histories in a range of geological contexts (e.g., Crowhurst et al., 2002; Reiners et al., 2003; Hendriks and Redfield, 2005; Stock et al., 2006; Thomson et al., 2010; Gautheron et al., 2012). The AHe age reflects the retention of helium produced by U-Th and Sm alpha decay within the crystal, which is controlled by diffusional loss over its thermal history. The first studies of ^{4}He diffusion in apatite assumed a constant diffusion behavior (Zeitler et al., 1987; Lippolt et al., 1994; Wolf et al., 1996; Farley, 2000). ^{4}He retention in apatite crystals was assumed to be characterized by "standard kinetics" controlled by activation energy, frequency factor, crystal size and thermal history (Wolf et al., 1998; Reiners and Farley, 2001), but subsequent work has demonstrated that other factors also need to be considered (e.g., Green et al., 2006; Green and Duddy, 2006; Hansen and Reiners, 2006). Recent data have indicated that radiation damage generated by U and Th decay can create traps for ^{4}He atoms, increasing ^{4}He retention as a function of the number of traps (Green and Duddy, 2006; Shuster et al., 2006). This radiation damage anneals with temperature (Chaumont et al., 2002) and the amount of damage in an apatite crystal is a balance between production and annealing, controlled by U-Th concentration and the thermal history respectively (Flowers et al., 2009; Gautheron et al., 2009; Shuster and Farley, 2009). The standard diffusion kinetics based on Durango apatite predicts a closure temperature of ~70 °C for a 70 μm radius apatite crystal cooling at 10 °C/Myr, and the He-PRZ (Partial Retention Zone) ranges from ~40 to 80 °C (Farley, 2000). According to the measurements of

Shuster et al. (2006), a damage-free apatite has a closure temperature closer to ~55 °C, and can range up to 110 °C or higher for a highly damaged apatite.

However, the raw age of any crystal may also be affected by other factors and processes such as zonation, ejection, and implantation from neighboring minerals. The long alpha stopping distance causes a significant depletion in ^{4}He concentration across the outer ~20 µm of an apatite crystal, creating a concentration gradient in the vicinity of the crystal surface. The alpha ejection correction (F_T) proposed by Farley et al. (1996) and refined by Ketcham et al. (2011) accounts for the ^{4}He loss by ejection out of the crystal. More detailed alpha ejection factors that account for zoned U-Th-Sm distributions (F_{ZAC}), have also been determined (Hourigan et al., 2005), but neither the F_T or F_{ZAC} corrections account for the effect of the ejection induced concentration gradients on diffusional loss. Some authors have asserted that this omission leads to an overcorrection of the ^{4}He age (Meesters and Dunai, 2002; Herman et al., 2007), but the interplay between ejection, damage and diffusion remains poorly quantified. Here we investigate the extent to which ejection affects diffusion using both standard and damage-modified kinetics. Zonation mapping is not a routine technique in (U-Th)/^{4}He thermochronology, although it has been developed and applied to some cases (Boyce et al., 2006; Herman et al., 2007; Dobson et al., 2008; Vermeesch, 2012). Therefore, although we present simulations on zoned crystals, these should be considered as an estimation of the potential effect of zonation, when it is neglected in the derivation and interpretation of the age. However if techniques probing the volumetric distribution of the concentrations of parent nuclides and ^{4}He become more routinely applied, then three-dimensional (3D) calculations such as those demonstrated in this paper can be potentially used to provide an accurate description of diffusion in such cases.

In addition to the helium generated within an apatite crystal, several studies have revealed that neighboring U-Th-Sm-rich crystals can be a source of external helium, with

95 implantation resulting from the long stopping distance of the energetic alpha particles
96 (Hourigan et al., 2005; Herman et al., 2007; Spiegel et al., 2009). The principal focus of
97 previous studies has been the quantification of ^{4}He injection, while omitting the role of the
98 subsequent diffusion on the AHe age. This is because such a calculation requires a full 3D
99 treatment of diffusion, as the location of the external sources precludes geometrical
100 symmetries. We use the 3D diffusion Monte Carlo Code developed in Gautheron and Tassan-
101 Got (2010) to quantify the combined effect of implantation and diffusion, and the impact on
102 the (U-Th)/He age in realistic situations and thermal histories. Abrasion, the process of
103 removing of the outermost 20 μm of the apatite corresponding to the range of the possible
104 implanted α-particles, has been suggested as a way to reduce the impact of implanted crystals
105 on AHe data sets (Spiegel et al., 2009). However, the full effect of abrasion on the ^{4}He age
106 distribution and on the fraction of implanted ^{4}He remaining after abrasion has not been
107 investigated. We assess how abrasion of the outer portion of the crystal can be used to
108 mitigate the impact of ejection, implantation and zonation in real samples, even where
109 significant diffusion has occurred. At the same time, we evaluate the extent to which thermal
110 history information may be obscured or lost by abrasion.
111
112 **2. Method**
113 The simulations presented in the following are based on the 3D Monte Carlo diffusion
114 code developed by Gautheron et al. (2006) and Gautheron and Tassan-Got (2010). The
115 flexibility of this approach makes it the ideal tool to fully describe ejection and diffusion for
116 homogeneous and heterogeneous ^{4}He distributions caused by α-emitter zonation, and variable
117 radiation damage. We have extended the 3D geometric module to allow the addition of any
118 number of possible external sources of alpha particles. For simplicity, the shapes of these
119 external sources are limited to spheres, ellipsoids, cylinders or rectangular boxes, and a

volumetrically uniform distribution of emitters is assumed for each, however the code can be extended to accommodate any geometry. The "strength" of each source is given by the ratio of emitter numbers or emitter concentrations. This implementation allowed us to simulate the alpha implantation from one crystal to another, and to simulate diffusion of implanted ^{4}He concentration profiles. Although the results of this contribution are based on illustrative examples taken from apatite ^{4}He thermochronology, the code can be applied to other systems. Similarly, our code is capable of simulating any crystal geometry; although here we report data for pyramidally terminated hexagonal prisms only. The code that accommodates U-Th zonation is available and can be downloaded from http://hebergement.u-psud.fr/flojt.

To assess the influence of diffusion, ejection, zonation and implantation on ^{4}He ages, we use four characteristic thermal histories (Fig. 1) similar to those used in a previous work (Wolf et al., 1998; Gautheron et al., 2009). These histories are representative of typical geological contexts: fast cooling followed by a long residence at the surface (H1), slow monotonic cooling (H2), heating and cooling during burial (H3), and long residence at 60 °C in the He partial retention zone (H4).

2.1. Alpha ejection and diffusion kinetics

All alpha particles are assumed to come from ^{235}U, ^{238}U and ^{232}Th chains in secular equilibrium. For crystals with a homogenous U-Th distribution the radioactive emitters are randomly scattered in the volume, and the direction of alpha emission is sampled randomly according to a uniform distribution. The stopping distance of each particle and the ending point of its trajectory are computed based on individual particle energy (Ziegler et al., 1985). In all cases we assume [Th]/[U]=1 but the results are not sensitive to this parameter. Under these conditions the mean stopping distance of the alpha particles is 19.7 µm whereas the range of the most energetic alpha in the chains is 41.2 µm. The emitters are randomly scattered through the volume with a weighted concentration representative of zonation, and

10^7 events are generated to follow each geometrical configuration and thermal history. The zonation of parent nuclides is implemented as shells of constant concentration, and constant distance from the surface of the grain, imposing a variation in concentration along the core-surface profile. 10^7 decay events are generated for each geometrical configuration and thermal history.

He diffusion was modeled using the coefficients for Durango apatite (Farley, 2000), except when investigating the effect of radiation damage, where we used the appropriate damage-controlled diffusion models and parameterizations (Green et al., 2006; Shuster et al., 2006; Flowers et al., 2009; Gautheron et al., 2009; Shuster and Farley, 2009). When damage-affected diffusion is simulated for zoned crystals the zone specific local level of damage is computed, and so the diffusion coefficient has a spatial variation within the grain.

2.2. Implantation

To investigate α-implantation into apatite, we placed alpha-emitting crystal(s) with 3D geometries and arbitrary U and Th concentrations in the volume surrounding the apatite crystal, and used Monte Carlo stochastic events to model alpha implantation, ejection and diffusion. No radiation damage due to ^{4}He implantation has been introduced in the simulation. 4×10^5 events were generated to compute the age that would be measured after 100 Ma, and $1\text{x}10^7$ events were generated for the computation of the ^{4}He concentration maps. In order to concentrate on the effect of diffusion on implanted ^{4}He, we restrict the configurations to simplified external source geometries, and for crystals with no radiation damage (produced by in-situ alpha-recoil damage), although our model can easily be applied as well to damage-specific kinetics and to more complex geometries. In any scenario the key quantity is not the number of decays in the external sources, but the emitter concentration close to the surface facing the apatite relative to the emitter concentration within the apatite, as only particles emitted within one stopping distance from the apatite surface can be implanted. In the

simulation the implantors are modeled as zircons with a density of 4.65 g.cm^{-3}, and an average stopping distance of 13.6 µm. A more accurate stopping distance for zircon is 16.3 µm, however for calculation simplicity the stopping distance is determined by a scaling law according to the density using: R=19.7×3.2/4.65=13.6 µm. When an alpha particle crosses a boundary we assume no energy loss as the alpha particle crosses the boundary, and once in the apatite the remaining stopping length scales according to the density.

2.3. Abrasion

To assess the effect of abrasion on non-implanted crystals, we used a modified version of the HeFTy software (Ketcham, 2005), which simulates the removal of some outer portion of a spherical crystal immediately prior to age determination. From a practical viewpoint abrasion is a complex process leading to a removal of the outer part of grains. This process rounds the sharp ridges of the crystal and it is neither constant in depth nor homomorphic, reducing more efficiently the elongated shapes to make them more compact. Larger volumes are removed from the terminations, reducing elongated shapes to more compact, equant geometries. It is beyond the scope of this work to model the details of the abrasion process. We instead provide the coded options for typical abrasion patterns: i) constant depth abrasion, ii) directional dependent abrasion leading to aspect ratio reduction, iii) ellipsoidal final shape to mimic a longstanding abrasion leading to a fully rounded shape, and present results for constant depth abrasion and iiii) abrasion along one facet of the crystal.

In the simulations the age is obtained by counting the helium and the emitter nuclides located inside the abraded volume at the end of the thermal history, whereas diffusion acted in the entire volume of the grain. We investigate the effect of abrasion on both isolated and implanted crystals.

3. (U-Th)/He age determination

To evaluate the influence of long alpha stopping distances on diffusion, we must first establish an appropriate reference frame. For any time-temperature path we define the "ejection-free" age (A_{EF}) as the age that would be measured if no ejection had occurred, i.e. all alpha particles have a stopping distance of zero. The A_{EF} depends on the time-temperature path and the shape and size of the crystal, but ignores the impact of ejection or implantation. This is the physical picture that underlies Dodson's (1973) equations for closure temperature.

Alpha particle ejection depletes ^{4}He from the margin of a crystal, diminishing the concentration at the crystal edge thereby lowering the rate of diffusion. Ejection therefore decreases the diffusive loss of helium (Farley, 2000). The alpha ejection correction (Farley et al., 1996; Ketcham et al., 2011) accounts for this ejection-controlled ^{4}He loss out of the crystal, but does not account for the effect of the concentration gradient on diffusional loss. A measured (U-Th)/He age (defined here as raw age) that is F_T-corrected will always be older than the ejection-free age except where cooling was instantaneous (because no diffusion occurred). In the context of the Dodson (1973) schema the utilization of the F_T correction increases the closure temperature.

This effect was noted by Meesters and Dunai (2002), and quantified using the equivalent sphere diameter to allow a simple 1D modeling approach (DECOMP). Here we fully calculate the effect for crystals with a homogenous or heterogeneous alpha-emitter distribution using our 3D Monte Carlo model, before applying it to radiation damaged crystals. In the following discussion raw ages are calculated in the model by counting the number of alpha particles within the apatite crystal volume at t = 100 Ma. This age results from simultaneous alpha ejection and diffusion, and includes all the additional effects of zonation and implantation when present.

The F_T correction has been defined for uniform single crystals (Farley et al., 1996) and for zoned single crystals (Hourigan et al., 2005) (F_{ZAC}, zonation averaged correction). We extend the definition to include implanted and abraded crystals, We denote as n_e the number of alpha particles produced by the analyzed grain volume (which may have been reduced by abrasion); n_s the number of alpha particles produced by the entire grain and stopped within the portion remaining after abrasion; and n_d the number of alpha particles remaining in the volume remaining after abrasion and after the diffusion process irrespective of their origin (native or implanted). In all situations the ejection-correction factor (denominated F_{ZAC} for the general case and specialized as F_T for uniform distribution) is the ratio of the number of alpha particles stopped in the analyzed mineral (before diffusion) divided by the number of alpha emitted from the same volume, whether zonation or implantation are present or not. Therefore $F_{ZAC}=n_s/n_e$. By definition this correction factor is intrinsically attached to the grain, its geometry and zonation, but it is independent of the thermal history and of its neighborhood. In particular it is not affected by implantation.

The raw age A is calculated from the ratio: $\rho= n_d/n_e$ by solving equation 1:

$$\rho = \frac{\sum_i n_i N_i (1-e^{-\lambda_i A})}{\sum_i n_i N_i (1-e^{-\lambda_i t})} \qquad \text{(Eq. 1)}$$

where the n_i are the relative contents of the head-of-chain isotopes, N_i the number of emitted alpha particles along each chain of time constant λ_i, and t the duration of the history. When this duration is small compared to the shortest half-life, which holds in our case because the history length is 100 Ma long, the age reduces to $A=t\times\rho$. In all cases the F_{ZAC}-corrected age is obtained with the same procedure by replacing ρ by $\rho/F_{ZAC,}$ so that the ratio of raw to F_{ZAC}-corrected ages is equal to F_{ZAC} when the history duration is small.

The A_{EF} is obtained by imposing a null range for the alpha particles. We quantify the effect of alpha redistribution by comparing the relative difference between the A_{EF}, the F_{ZAC}-corrected age, and the raw age using:

$$Deviation\ (\%) = \frac{(A - A_{EF})}{A_{EF}} \qquad \text{(Eq. 2)}$$

where A is the F_T-or F_{ZAC}-corrected age or the raw age as defined above. All deviations are shown as percentages. When there is no diffusion (very rapid cooling) the F_T- or F_{ZAC}-corrected ages and the A_{EF} will be the same and the deviation vanishes.

4. The interaction between alpha ejection and diffusion for isolated crystals

4.1 Homogeneous alpha-emitter distribution

Ejection affects the ^{4}He profile in a crystal, and reducing diffusive loss. The ejection correction does not account for this reduction so when applied it leads to an overcorrection. Diffusion has been simulated for a realistic case: a regular hexagonal prism with two pyramids having a total length equal to 6 times the crystal radius (aspect ratio = 6). The simulation was performed for a range of crystal sizes and the deviation between the F_T-corrected age and A_{EF} is shown in Fig. 2A as a function of the crystal size represented by F_T and by the equivalent sphere radius. The deviation always vanishes at large sizes because the depleted edge becomes volumetrically insignificant (i.e. F_T approaches to 1). For rapidly cooled samples (H1), the deviation stays within 3 % of the $A_{EF,}$ and reflects the small amount of diffusion that is expected to occur at 20 °C (Fig. 1); with a lower model surface temperature, the deviation would be even lower. As the cooling rate reduces (H2), the crystal spends a significant portion of its history in the He-PRZ and the deviation increases to 7-8 %. For the scenarios H1 and H2 the size dependence of the deviation remains approximately

267 monotonic whereas for H3 and H4 (scenarios with reheating and long residence at 60 °C, Fig.
268 1) a maximum is reached before the deviation levels off at small sizes. This trend can be
269 understood by considering the diffusional length scale, $l_d = \sqrt{\int Ddt}$ which represents depth
270 to which the concentration is affected by diffusion. When it becomes of the order of the grain
271 size, and the residence time in the PRZ is long (which is the case at small sizes for H3 and
272 H4, and to a lesser extent for H2), diffusion acts on the bulk of the grain. When this is the
273 case, the diffusion in the outermost volume where ejection reduces diffusion plays a less
274 prominent, though still significant role (at some 6-8%).

275 The deviation of the raw age from the A_{EF} is shown in Fig. 2B. Deviations reach up to
276 -30 % for small crystal sizes (R_s=40 μm), and for typical apatites (F_T from 0.7 to 0.85) the
277 deviation ranges from -10 to -25 %. The deviation from the A_{EF} are much higher and the
278 opposite sense to those for the F_T-corrected age, even when diffusion is strong. Similar
279 simulations for simpler geometries yield similar results (Meesters and Dunaï, 2002). This
280 shows that although diffusional losses do not scale with the F_T factor when alphas are ejected,
281 the F_T-corrected age is good approximation of age that would be recorded if no ejection had
282 occurred (A_{EF}).

283 As the closure temperature evolves with the amount of radiation damage accumulated
284 within a crystal, the amount of radiation damage can have a major impact on ages obtained
285 from samples that have experienced thermal histories with reheating (e.g. H3) (Gautheron et
286 al., 2009). To assess the robustness of the F_T-corrected age we subjected crystals of the same
287 geometry but different effective uranium eU concentrations: 10, 20, 50 and 100 ppm to the
288 reheating scenario (H3), with Tmax = 70°C (Fig. 3) Contrary to the standard kinetics case,
289 when the creation and annealing of damage is taken into account for the diffusivity using the
290 Gautheron et al. (2009) model the deviation remains monotonic, increasing steadily for small
291 grains. This is a consequence of the higher retentivity and of a diffusion length remaining

292 smaller than the grain size. This increase of the retentivity is specific to the model from
293 Gautheron et al. (2009) where the production of damage is proportional to eU. For eU larger
294 than 30 ppm, the results will differ strongly with those obtained from the Flowers et al. (2009)
295 model. In the latter case for eU < 25 ppm the result will be similar to standard kinetic model,
296 and for higher eU, the AHe will start to increase. In addition when eU increases the diffusion
297 is almost frozen and becomes closer to a no-diffusion case where the F_T-correction is very
298 accurate. This explains the order of the curves in Fig. 3. We observe that the deviation of the
299 F_T-corrected age is higher when using the damage model, reaching 5 to 9 %, for typical
300 crystal sizes. However it remains much lower than the deviation of the raw age, and the
301 conclusion based on the standard kinetics still holds.

302 **4.2 Heterogeneous ^{4}He content due to U-Th zonation**

303 As with the homogeneous case, when diffusion has occurred the application of the F_T
304 or F_{ZAC} correction factors do not account for diffusive ^{4}He loss from the crystal. Our model
305 allows the effect of simultaneous diffusion and ejection to be investigated for zoned samples
306 of any crystal and zonation geometry. As already mentioned we adopted a shelled distribution
307 for the emitter parents. We considered again a pyramided hexagonal prism but the size is
308 fixed: 300 µm in height (including the pyramids) and 50 µm for the radius of the basal
309 section, corresponding to F_T=0.754 and R_S=57.3 µm. We implemented an outer layer of
310 constant thickness of 20 µm from the surface, denominated the rim, and an internal one
311 encompassing the rest of the grain, called the core. The adoption of such a geometry and a
312 thickness of the rim which is close to the mean stopping distance are well suited to explore
313 the impact of ejection on diffusion. Although the thickness of the outer layer is less than half
314 of the radius the rim accounts for 75 % of the total volume. The F_{ZAC}-corrected helium age is
315 calculated by our model for a standard kinetic He diffusion and the deviation from A_{EF} is
316 shown in Fig. 4A as a function of the rim U-Th concentration ratio (C_{rim}/C_{core}). A value equal

317 to 1 of this ratio represents uniform distribution. The age deviates in a similar manner to that
318 seen for the homogeneous examples but with a strong additional dependence on the
319 concentration ratio. When the rim is enriched ($C_{rim}/C_{core} > 1$) the age is older than A_{EF} for the
320 same reasons as in the uniform case but the deviation is enhanced by the fact that the age
321 becomes more sensitive to the surface region, which is mostly affected by ejection. The gap
322 levels off when the helium budget in the core becomes negligible compared to the total
323 helium content and it reaches 10-12 % for the scenarios dwelling a long time in the He-PRZ
324 (H2, H3 and H4), whereas it is limited to 3 % for the fast cooled scenario H1. In the case of
325 highly depleted rims ($C_{rim}/C_{core} < 0.1$) the deviation becomes negative, meaning that ejection
326 helps the helium to flow out by diffusion. This may appear as paradoxical but it can be
327 understood by the injection of alphas emitted from the core into the rim from where it is more
328 easily evacuated by diffusion because it is closer to the surface. One can see however that the
329 F_{ZAC}-corrected age is more accurate for depleted rims as the deviation is limited to ~ -5 %
330 (Fig. 4A). Similarly to the uniform distribution case, we look at the effect of the increased
331 helium retention when damage affects the diffusivity. For the H4 scenario, which maximizes
332 the impact of diffusion, we plot the deviation on the F_{ZAC}-corrected age in Fig. 4B for a set of
333 eU concentrations. Those concentrations are averages over the entire grain volume V_0
334 whereas the local concentrations in the rim and in the core are dependent of C_{rim}/C_{core} so that:
335
336 $$eU = \left(C_{rim}V_{rim} + C_{core}V_{core}\right)/V_0 \quad \text{(Eq. 3)}$$
337
338 As the eU concentration is zone-dependent the level of damage depends on the zone
339 too, so that the diffusion coefficient gets discontinuities at the zone boundaries and also the
340 ^{4}He concentration gradient. When this problem is handled by solving the diffusion equation a
341 special care should be taken because the Laplacian form of Fick's equation is no longer valid,

but with the Monte Carlo method it is merely treated by conserving the velocity of the atom crossing the boundary and scaling the mean free path according to the diffusion coefficient (Gautheron and Tassan-Got (2010).

The shape of the dependences on C_{rim}/C_{core} is similar to the standard diffusion case (Fig. 4B) and for $C_{rim}/C_{core} > 0.3$ the deviation drops for the highest eU contents, reflecting the blocking of diffusion. In particular for enriched rims and for eU contents larger than 10 ppm, the F_{ZAC}-corrected age deviation remains comparable to the uniform case (< 6 %). However, for strongly depleted rims ($C_{rim}/C_{core} < 0.2$), the deviation decreases significantly down to ~15%. Again this is due to the injection of alphas from the core into the rim where diffusion is very efficient because it is damage-free.

Although our model can calculate the zonation dependent F_{ZAC} correction for any crystal geometry and parent nuclide distribution, it can only be accurately determined when the distribution is known. In most AHe studies the zonation pattern is not measured and is assumed to be uniform. It is worth assessing the error introduced when one ignores the zoned distribution and makes this uniform assumption. For this purpose we compare the ages obtained for two crystals, one zoned and one uniform, for each of the four thermal histories, and we assume that any information on zonation is unknown so that we apply the same F_T correction to both crystals. The ratio of the two ages is displayed in Fig. 5A as a function of the rim enrichment for the zoned grain. We find that as soon as the C_{rim}/C_{core} ratio departs by a factor 2 from homogeneity a significant error affects the age determination, beyond the analytical error. The most critical situation is for depleted rims where the error reaches 50 % for samples having experienced a long-stay in the He-PRZ. One may raise the question of the origin of this problem: diffusion acting differently or wrong ejection correction. The answer can be guessed from the behavior of the H1 trend in Fig. 5A, which is affected also by a large error (30 %) in spite of the almost frozen diffusion for this scenario. This is confirmed by

applying the appropriate F_{ZAC} correction to the zoned crystal and Fig. 5B shows that in this case the error is significantly reduced. This shows that the loss of information on zonation can lead to severe difficulties in the interpretation of ages. However this is not a matter of diffusion, which is moderately affected by the mapping of parent emitters, but rather a problem of assessment of the ejection correction. Of course this difficulty dies out for large grains as this correction gets close to 1.

5. The interaction between alpha ejection and diffusion for implanted crystals

5.1. Implantation from a single external source

Our initial model places a zircon with eU of 1000 ppm close to an apatite crystal with eU of 20 ppm (Fig. 6). The zircon is modeled as a squared prism 100 µm length and 60 µm width, and is placed parallel to the apatite crystal at a distance of 2 µm. The apatite is modeled as a hexagonal prism terminated by two pyramids with radius of 50 µm and a total length of 300 µm (Fig. 6A). When solving the diffusional evolution the small layer of matter between the apatite and its neighboring zircon (2 µm) is enough efficient to absorb and drive entirely the ^{4}He atoms leaking from the apatite, either because it is highly diffusive or advective. It means that the role of the companion zircon is limited to implantation without any perturbation on the diffusion process. Figure 6 shows a cross section of the ^{4}He distribution within the apatite crystal, taken in the horizontal mid-plane of the apatite grain where the level of implanted alphas is expected to be maximal..

For a rapidly cooled sample (i.e. no diffusion) the model predicts a ~20×[He] enrichment in the vicinity of the zircon crystal (Figs. 6B,D). Figure 6D clearly shows the implantation front at the apatite-zircon boundary and the usual ejection profile at the opposite crystal edge. For the thermal history scenario where this crystal has experienced the maximum time within the partial retention zone (H4) we observe an order of magnitude

reduction in the ^{4}He concentration in the implantation peak caused by enhanced diffusion at the crystal surface, and the peak becomes less sharply defined (Figs. 6C & D). It is apparent that diffusion significantly affects both the ^{4}He pattern and the total ^{4}He content of the crystal.

The increase in ^{4}He age caused by the implantation has been calculated as a function of the eU concentration in the external source (0 to 1000 ppm) (Fig. 7), for each of our four thermal histories. For the rapidly cooled sample (H1), in the most severe case of eU contrast implantation would yield an AHe age up to 60 % older than for an isolated crystal. For the slowly cooled sample (H4) (e.g. Fig. 7) the AHe age is ~50 % older. For any scenario, implantation from a single crystal of typical zircon (eU=200-500 ppm) in close proximity will increase the measured ^{4}He age by a minimum of 10 to 20 %. It is clear that if external sources of differing eU concentrations cause implantation into different apatite crystals the resultant data set would have very poor age reproducibility.

5.2 Implantation from multiple external sources

An apatite may have more than one U-Th rich neighbor, or a relative eU range this is more extreme than those represented above. To place a boundary on the possible age dispersion resulting from more extreme implantation we examined a situation where the apatite crystal is surrounded by several zircons. All external sources are 100 µm in length, and except for one source, they lie parallel to the apatite crystal faces (Fig. 8A & B). All external sources have the same emitter concentration. The apatite crystal geometry and the location of the cross section showed in Figure 8 are the same.

The complex implantation front caused by contributions from multiple sources is shown in Figure 8. For this apatite, with eU=20 ppm and external sources with eU=1000 ppm, only small sections of the apatite do not experience implantation (e.g. the left lower corner). As in the previous example, the slowly cooled sample exhibits higher concentrations and more strongly enhanced core-rim concentration profiles (Fig. 8A) than for the slowly cooled crystal

(H4, simultaneous redistribution and diffusion) (Fig. 8B). The measured age of these crystals is again plotted against the external source emitter concentration for each of the four thermal histories (Fig. 8C). Assuming a relative emitter concentration [$eU_{external}/eU_{apatite}$] of 50, as shown in Fig. 8C, implantation increases the measured AHe age by up to ~280 % for rapidly cooled samples, and ~230 % for the slowly cooled crystals. Even at more modest external source eU concentrations (~200 ppm), the AHe ages are ~30-40 % higher than for an isolated crystal. For abraded grain, a significant amount of 4He can have diffuse inside the crystal, and the AHe age will so still be affected.

5.3. Generalization about implantation from external sources

As the impact of implantation on the age is highly dependent on the neighborhood, number, geometry, enrichment of the sources, it was interesting to find a simple parameter carrying the strength of the implantation and quantifying the perturbation on the age. As a tentative approach we tested the ratio of the amount of implanted ^{4}He in the apatite to the amount internally produced in the grain, which we denominate as native. The ^{4}He age is compared to a non-implanted grain of same geometry and size, as a function of [He] implanted / [He] native, superimposing the data of the two geometrical configurations: single and multiple implantors. The results are reported in Fig. 9, where the red symbols represent implantation from single external sources, and the black symbols represent multiple implantation sources. The striking feature is that for a given temperature history the points follow the same linear trend, independently of the geometry, indicating that the implanted/native ratio captures the full complexity of geometrical effects. A ratio [He] implanted / [He] native = 2 corresponds to an emitter eU=1000 ppm in case of the particular multiple source configuration used in the previous subsection. It would correspond to eU=2900 ppm for the single source configuration described in 5.1.

441 In conclusion, although a full calculation can be carried out as we showed in this
442 section, a single generic geometrical configuration can be selected arbitrarily as representative
443 of the different situations to extract the dependence of the age on the ratio [He] implanted /
444 [He] native, and this leads to a simplification of the simulations.
445

6. The effect of abrasion

6.1 Isolated crystals

Even for homogeneous, isolated crystals ^{4}He is depleted at the crystal edge by ejection and diffusion, and abrading any crystal to remove this depleted zone therefore increases the concentration of ^{4}He per unit of crystal volume, and by extension the calculated ^{4}He age. To quantify the magnitude of this effect we inspected a set of 100 Myr thermal histories that feature reheating, with sequentially higher peak burial temperatures (Fig. 10A), using the new abrasion functionality in HeFTy. Modeling spherical apatite crystals with radii of 60, 80 and 100 µm, and the using diffusion kinetics of Farley (2000) (non-radiation damaged crystals), we quantify the age increase caused by abrading 0, 20 and 25 µm uniformly from the crystal surface. All models incorporate simultaneous ejection and diffusion. The ages from the un-abraded crystal are shown with F_T correction, and the ages of abraded grains are uncorrected. If we consider the case of a 60 µm crystal in more detail (Fig. 10B), we see the predicted increase in age with the abrasion volume. Interestingly, the abraded crystals show no significant age reduction at all due to reheating until burial temperature exceeds 40 °C (Fig. 10B), whereas the non-abraded crystal experiences an 8 % F_T-age reduction at that temperature. The abraded crystal ages then reduce more rapidly as the peak temperature approaches the level required for resetting the AHe system. It is also noteworthy that the abraded ages are always older than the F_T-corrected ages of the non-abraded crystals, in essence making the net result of abrasion an even more severe "overcorrection" than using F_T.

Figures 10C & 10D show the relationship between percentage age increase and abraded volume for different crystals sizes and maximum temperatures. With a 20 µm abrasion the age rises up to 2-20 % with heating from 20-60 °C, then falls as the degassing by diffusion becomes more efficient and the thermochronometer is reset. Increasing the abraded volume by a further 5 µm increases the measured ages by up to an additional ~3-4 %. The crystal size

dependence of the age increase means that the ages of abraded crystal should not be expected to reproduce in reburial scenarios. Furthermore as the accurate measurement of the abraded volume is not straightforward, and our results indicate that for these thermal histories, dispersion on the order of 0.5-1 % will be added per micrometer error in the measurement of the abraded volume in this idealized scenario, and probably by a somewhat larger margin if the full complexity of abrasion is accounted for.

6.2 Implanted Crystals

The effect of abrasion on the measured ^{4}He ages of crystals that have experienced implantation was assessed by recalculating the total ^{4}He concentration in both the isolated and implanted crystal after a 20 μm thick shell had been removed. For rapidly cooled samples (H1) only the highly energetic alphas of the Th chain will penetrate more than 20 μm into the apatite crystal, and so the implanted ^{4}He remains mostly in the outer 20 μm. After abrasion the implanted crystal contains approximately 4 % more ^{4}He than the isolated crystal, compared to 60 % excess before abrasion. For the samples that experienced slower cooling and long residence in the He partial retention zone abrasion does not remove all the implanted He. For the monotonic slow cooling sample (H2), the excess ^{4}He within the crystal is reduced from ~60 % to ~10 % by abrasion, and for the intermediate histories (H3, H4) the excess ^{4}He is reduced from ~50 % to ~13 % and ~45 % to 12 % respectively (Fig. 7). In all scenarios abrasion has significantly reduced the age dispersion of the sample. For the crystals with stronger implantation caused by multiple external sources (Fig. 8,9), abrasion also causes implanted and isolated crystals to yield more comparable ages. The higher amount of implanted ^{4}He results in a stronger inward diffusion. Consequently the abraded crystals that have experienced some degree of diffusive loss retain a higher proportion of the excess He: up to ~35 %, in contrast to the ~13 % for the abraded that experienced implantation from a single emitter. The point at which the excess ^{4}He retained after abrasion exceeds 8 % (i.e.

(higher than the age reproducibility of (U-Th)/He dating standards) occurs, for the multiple source cas, when the external source concentration exceeds ~200-300 ppm (i.e. 10 x that of the apatite) for the slowly cooled samples, but is ~700 ppm for the rapidly cooled samples. The duration over which inward diffusion occurs controls the excess ^{4}He measured after abrasion; hence the slow diffusion monotonic cooling history (H2) requires higher concentrations than H3 & H4. The limiting source concentrations mentioned above are dependent on the details of the geometry, but they can be expressed in a more universal way through the ratio of implanted/native helium. This ratio should stay below 1.5 for rapidly cooled samples, and below 0.5 for samples, which have undergone diffusion in the He-PRZ (Fig. 9B).

7. Implantation & abrasion: implications for (U-Th)/He thermochronology

In agreement with earlier studies (Spiegel et al., 2009), our results have shown that the effect of alpha implantation on ^{4}He ages is significant. We also show that for slowly cooled samples, inward diffusion of implanted ^{4}He can significantly affect the helium age, even if the outer ~20 μm of the crystal is abraded. However, it is evident that in most cases the ^{4}He age dispersion due to implantation can be reduced to a level comparable with typical age reproducibility (~8 %). Age dispersion that survives abrasion may be taken as evidence of extended time in the He-PRZ, although this signal may be ambiguous given other dispersion-causing features (such as zoning) and would require independent corroboration. However, abrasion should be used with caution. We have shown that the precise determination of the amount of material that has been abraded in the 20-25 μm range from a crystal will only contribute a second-order source of error, but abrasion of a 20 μm shell reduces the crystal volume by between 30 % (r=200 μm) and 90 % (r=40 μm). For the crystal sizes typically analyzed for (U-Th)/He this volume reduction will significantly increase the uncertainty in the

U, Th and ^{4}He measurements. For smaller crystal significant dispersion will also be introduced by the uncertainty in the abrasion volume. Furthermore, the measured age from an abraded crystal will also be older than an un-abraded crystal for a given thermal history, and the abraded age should therefore not be considered as, or confused with an "ejection-free age". The outermost region of the crystal is the region sensitive to the low-temperature part of the thermal history (<40 °C), an so while augmentation of computational methods to incorporate data from implanted and abraded crystals into the thermal history simulations; removing this rim explicitly and irrevocably loses thermal history information.

8. Conclusions

This contribution focuses on the interplay between ejection, implantation and diffusion and their effect on the (U-Th)/He ages recorded by an individual apatite crystal during passage through the He partial retention zone. The 3D Monte Carlo code developed here fully models simultaneous ejection and diffusion for any crystal and zonation geometry, and for any number of external alpha emitting sources. We have presented examples of external alpha emitting sources with simple euhedral geometries, but more realistic geometries can be modeled. We discuss the use of the F_T (homogeneous eU content) and F_{ZAC} (heterogeneous eU content) correction for homogeneous, zoned and radiation damaged crystals and conclude that applying the F_T or F_{ZAC} correction introduces minimal error in correcting for (U-Th)/He ages for ^{4}He loss. Although diffusional losses do not scale with the ejection factor when alphas are ejected, the F_T- F_{ZAC}-corrected age is good approximation of age that would be recorded if no ejection had occurred (A_{EF}). We therefore recommend that F_T- or F_{ZAC}- correction, as defined by Ketcham et al. (2011), be routinely employed when He ages are compared against each other and other thermochronometers, although for inverse

545 modeling the raw age is generally the required input parameter. But the loss of information on
546 the zonation mapping when it is present may lead to large errors in case of enriched cores.

547 Using the unique ability of our model to fully investigate internal and external
548 influences on ^{4}He redistribution (ejection and diffusion from multiple crystals) we have
549 quantified the change in measured (U-Th)/He age introduced by implantation. Our data show
550 that for implantation by a single external source with 20× higher eU, the implanted crystal can
551 have ~60% excess He. For more extreme cases where an apatite is surrounded by multiple
552 external sources the excess ^{4}He can be > 250-300%.

553 Our models also quantify the effect of abrasion on implanted and isolated crystals,
554 highlighting the ability of abrasion to significantly reduce (U-Th)/He dispersion. For slowly
555 cooled samples the reduction is not complete and implanted crystals can still contain 10-30 %
556 excess He. We demonstrate that for one or multiple sources, and for any kind of distance from
557 the crystal to the source, the only important parameter is the implanted/native He content.
558 With the access to this value, the AHe age deviation can be determined for natural or abraded
559 crystals. We suggest that abrasion should still be used with caution because of the
560 uncertainties, biases, and information loss introduced even in the case of uniform distribution
561 without external implantation.

562 Although many of the variables that can affect (U-Th)/He ages are impossible to
563 determine using current analytical techniques, or are not routinely measured (e.g. zonation,
564 implantation), with fully 3D modeling techniques such as those presented here, it is now
565 possible to identify and quantify the causes of age dispersion and improve our understanding
566 and interpretation of (U-Th)/He data.
567

Acknowledgments:

Andy Carter and Peter van der Beek are thanked for constructive discussions during the manuscript preparation. This work is part of the ANR06-JCJC-0079 project granted to C. Gautheron, and was written during the CNRS sabbatical year at ISTerre, Grenoble (2011-2012) of C.G. Damien Barbosa is thanked for the great jobs done for the F_T-ejection and abrasion software. The Manchester X-ray Imaging Facility, which was funded in part by the EPSRC (grants EP/F007906/1, EP/F001452/1 and EP/I02249X/1).

References:

Boyce, J.W. Hodges, K.V., Olszewski, W.J., Jercinovic, M.J., Carpenter, B.D., Reiners, P.W., 2006. Laser microprobe (U-Th)/He geochronology, Geochim. Cosmochim. Acta. 70, 3031-3039.

Chaumont, J., Soulet, S., Krupa, J.C. and Carpéna, J., 2002. Competition between disorder creation and annealing in fluoroapatite nuclear waste forms. Journal of Nuclear Materials, 301: 122-128.

Crowhurst, P., Green, P.F. and Kamp, P.J.J., 2002. Appraisal of (U-Th)/He apatite thermochronology as a thermal history tool for hydrocarbon exploration: An example from the Taranaki Basin, New Zealand. AAPG Bulletin, 86(10).

Dobson, K. J., Stuart, F. M., Dempster, T. J., and EIMF, 2008. U and Th zonation in Fish Canyon Tuff zircons: Implications for a zircon (U–Th)/He standard. Geochim. Cosmochim. Acta 72, 4745–4755.

Dodson, M.H., 1973. Closure temperature in cooling geochronological and petrological systems. Contrib. Min. Petrol., 40: 259-274.

Farley, K.A., 2000. Helium diffusion from apatite: general behavior as illustrated by Durango fluorapatite. J. Geophys. Res., 105: 2903-2914.

Farley, K.A., Shuster, D. and Ketcham, R.A., 2011. U and Th zonation in apatite observed by laser ablation ICPMS, and implication for the (U-Th)/He system. Geochim. Cosmochim. Acta, 75: 4515-4530.

595 Farley, K.A., Wolf, R.A. and Silver, L.T., 1996. The effects of long alpha-stopping on (U-Th)/He
596 ages. Geochim. Cosmochim. Acta, 21: 4223-4229.
597 Flowers, R., Ketcham, R.A., Shuster, D. and Farley, K.A., 2009. Apatite (U-Th)/He thermochronology
598 using a radiation damage accumulation and annealing model. Geochim. Cosmochim. Acta, 73:
599 2347-2365.
600 Gautheron, C., Tassan-Got, L. and Farley, K.A., 2006. (U-Th)/Ne chronometry. Earth Planet. Sci.
601 Lett., 243: 520-535.
602 Gautheron, C., Tassan-got, L., Barbarand, J. and Pagel, M., 2009. Effect of alpha-damage annealing
603 on apatite (U-Th)/He thermochronology. Chem. Geol., 266: 166-179.
604 Gautheron, C. and Tassan-Got, L., 2010. A Monte Carlo approach of diffusion applied to noble
605 gas/helium thermochronology. Chem. Geol., 273: 212-224.
606 Gautheron, C. et al., 2012. Tectonic and basin-fill history of the central Peruvian Subandes foreland
607 (~12°S) viewed by apatite (U-Th)/He and fission track double dating. in review in Basin
608 Research.
609 Green, P.F., Crowhurst, P.V., Duddy, I.R., Jaspen, P. and Holford, S.P., 2006. Conflicting (U-Th)/He
610 and fission track ages in apatite: Enhanced He retention, not annealing behaviour. Earth
611 Planet. Sci. Lett., 250: 407-427.
612 Green, P.F. and Duddy, I.R., 2006. Interpretation of apatite (U-Th)/He ages and fission track ages
613 from cratons. Earth Planet. Sci. Lett., 244: 541-547.
614 Hansen, K. and Reiners, P.W., 2006. Low temperature thermochronology of the southern East
615 Greenland continental margin: Evidence from apatite (U-Th)/He and fission track analysis and
616 implications for intermethod calibration. Lithos, 92: 117-136.
617 Hendriks, B.W.H. and Redfield, T.F., 2005. Apatite fission track and (U-Th)/He data from
618 Fennoscandia: An example of underestimation of fission track annealing in apatite. Earth
619 Planet. Sci. Lett., 236: 443-458.
620 Herman, F., Braun, J., Senden, T.J. and Dunlap, W.J., 2007. (U-Th)/He chronometry: Mapping 3D
621 geometry using micro-X-ray tomography and solving the associated production-diffusion
622 equation. Chem. Geol., 242: 126-136.

623 Hourigan, J.K., Reiners, P.W. and Brandon, M.T., 2005. U-Th zonation-dependent alpha-ejection in
624 (U-Th)/He chronometry. Geochim. Cosmochim. Acta, 69: 3349-3365.
625 Ketcham, R.A., 2005. Forward and inverse modelling of low-temperature thermochronolgy data. In:
626 P.W.a.E. Reiners, T.A. (Editor), Low temperature thermochronology: techniques,
627 interpretations and applications. Reviews in mineralogy and geochemistry, pp. 275-314.
628 Ketcham, R.A., Gautheron, C. and Tassan-got, L., 2011. Accounting for long alpha-particle stopping
629 distances in (U-Th-Sm)/He geochronology: refinement of the baseline case. Geochim.
630 Cosmochim. Acta, 75: 7779-7791.
631 Lippolt, H.J., Leitz, M., Wernicke, R.S. and Hagedorn, B., 1994. (Uranium+thorium)/helium dating of
632 apatite: experience with samples from different geochemical environments. Chem. Geol., 112:
633 179-191.
634 Meesters, A.G.C.A. and Dunai, T.J., 2002. Solving the production-diffusion equation for finite
635 diffusion domains of various shapes Part II. Apllication to cases with a-ejection and
636 nonhomogeneous distribution of the source. Chem. Geol., 186: 347-363.
637 Reiners, P.W. and Farley, K.A., 2001. Influence of crystal size on apatite (U+Th)/He
638 thermochronology: an example from the Bighorn Mountains, Wyoming. Earth Planet. Sci.
639 Lett., 188: 413-420.
640 Reiners, P.W., Ehlers, T., Mitchell, S.G. and Montgomery, D.R., 2003. Coupled spatial variations in
641 precipitation and long-term erosion rates across the Washington Cascades. Nature, 426: 645-
642 647.
643 Shuster, D., Flowers, R. and Farley, K.A., 2006. The influence of natural radiation damage on helium
644 diffusion kinetics in apatite. Earth Planet. Sci. Lett., 249: 148-161.
645 Shuster, D. and Farley, K.A., 2009. The influence of artificial radiation damage and thermal annealing
646 on helium diffusion kinetics in apatite. Geochim. Cosmochim. Acta, 73(183-196).
647 Spiegel, C., Kohn, B., Belton, D., Berner, Z. and Gleadow, A., 2009. Apatite (U-Th-Sm)/He
648 thermochronology of rapidely cooled samples: The effect of He implantation. Earth Planet.
649 Sci. Lett., 285: 105-114.

650 Stock, G.M., Ehlers, T.A. and Farley, K.A., 2006. Where does sediment come from? Quantifying
651 catchment erosion with detrital apatite (U-Th)/He thermochronometry. Geology, 34(9): 725-
652 728.

653 Thomson, S.N. et al., 2010. Glaciation as a destructive and constructive control on mountain building.
654 Nature, 467.

655 Vermeesch, P., Sherlock, S.C., Roberts, N.M.W., and Carter, A., 2012. A simple method for in-situ U-
656 Th-He dating, Geochimica et Cosmochimica Acta, 79, 140-147

657 Wolf, R.A., Farley, K.A. and Silver, L.T., 1996. Helium diffusion and low-temperature
658 thermochronology of apatite. Geochim. Cosmochim. Acta, 60: 4231-4240.

659 Wolf, R., Farley, K.A. and Kass, D., 1998. A sensitivity analysis of the apatite (U-Th)/He
660 thermochronometer. Chem. Geol., 148: 105-114.

661 Zeitler P. K., Herczig A. L., McDougall I., and Honda M. (1987) U-Th-He dating of apatite: a
662 potential thermochronometer. Geochim. Cosmochim. Acta, 51, 2865-2868.

663 Ziegler, J.F., Biersack, J.P. and Littmark, U., 1985. The stopping and range of ions in solids.
664 Pergamon Press, 321 pp.

665 **Figure captions**

666

667 **Figure 1:** Time-temperature paths used to calculate He ages (modified after Wolf et al., 1998;
668 Gautheron et al., 2009). H1- (filled diamonds) rapid cooling followed by long residence at
669 20ºC; H2– (open diamonds) monotonic slow cooling; H3– (open squares) reheating; H4-
670 (filled squares) long residence in the He partial retention zone where diffusion is rapid.

671

672 **Figure 2:** The effect of ejection and diffusion on homogeneous crystals of regular hexagonal
673 geometry (variable radius and Height/Radius=6, terminated by two pyramids) for the thermal
674 histories in Fig. 1. Deviation of the calculated F_T-corrected (A) and the raw (U-Th)/He age
675 (B) from the ejection-free age, which is the one that would be measured if no ejection had
676 occurred, i.e. all alpha particles having a stopping distance of zero for a homogeneous emitter
677 distribution. The symbols are as for Fig. 1 Model uses hexagonal crystal geometry with F_T of
678 0.6-1 (40 μm < Rs < 200 μm), the diffusion kinetics of Farley (2000), and α-particles from a
679 decay chain with a mean stopping distance of 19.69 μm (Ketcham et al., 2011). The stopping
680 distance of each particle was explicitly calculated (see text for details).

681

682 **Figure 3:** Deviation of the calculated F_T-corrected for crystals of different [eU] contents and
683 sizes for the reheating thermal history (H3-Fig. 1). Similar hexagonal geometry as in Fig. 2
684 was used in the simulations. All crystals have a homogeneous emitter distribution. Model
685 parameters are as for Fig. 2, but the alpha-recoil damage and annealing model has been used
686 (Gautheron et al., 2009). Open squares - Durango diffusion kinetics (Farley, 2000); black
687 diamonds – eU=10 ppm; gray circles – 20 ppm; filled triangles – 50 ppm; crosses – 100 ppm.

688

689 **Figure 4:** The effect of ejection and diffusion on zoned crystals for the thermal histories in
690 Fig. 1. Deviation (in %) of the calculated F_{ZAC}-corrected age for a crystal for standard He
691 kinetics and for the four thermal histories (Diagram A) and for alpha-recoil damage in the
692 long stay in the He-PRZ H4 case (Diagram B), with a 20 µm rim, with $0.01 < C_{rim}/C_{core} < 10$.
693 Crystal geometry was a hexagonal prism, radius = 50 µm, total length = 300 µm, terminated
694 by two pyramids, zoned rim = 20 µm deep. Alpha particles are emitted by Th and U with
695 Th/U=1. Symbols are as for Fig. 1 in diagram A. For diagram B, model parameters are as for
696 Fig. 2 and 3.
697
698 **Figure 5:** The deviation introduced by assuming homogeneity when considering (A) the F_T-
699 corrected age and (B) the F_{ZAC}-corrected age of zoned crystals, for each of the thermal
700 histories as a function of eU rim/core ratio. The same crystal geometry and He stopping
701 distance are used as in Fig. 4. For comparison, the 8 % analytical error zone is shown.
702
703 **Figure 6:** Implantation from a single external source. (A) Model geometry, apatite eU=20
704 ppm, zircon eU=1000 ppm. Helium concentration after 100 Myr, for (B) rapidly cooled
705 crystal and (C) slowly cooled sample. (D) Helium concentration profiles across B (black) and
706 C (red). See text for full model geometry. Alpha particles are emitted by Th and U with
707 Th/U=1. Their mean range is 19.7 µm in the apatite and 13.6 µm in the zircon.
708
709 **Figure 7:** Fractional increase in He age caused by implantation as a function of external
710 emitter concentration for each of the thermal histories. (A) Entire crystal. (B) Abraded crystal.
711 Symbols are as for Fig. 2. Model geometry is as shown in Fig. 6. For comparison, the 8 %
712 analytical error zone is shown.
713

Figure 8: Implantation from multiple external sources. Model geometry and helium concentration after 100 Myr, for (A) rapidly cooled crystal and (B) slowly cooled sample. Apatite eU=20 ppm, all zircons eU=1000 ppm. Fractional increase in He age caused by implantation as a function of external emitter concentration for (C) entire crystal, and (D) abraded crystal for each of the thermal histories. Symbols are as for Fig. 1. See text for full model geometry. For comparison, the 8 % analytical error zone been reported.

Figure 9: Dependence of AHe age of an implanted grain, referred to an isolated grain, on the ratio of the implanted to native helium. (A) Entire non-abraded grain; (B) abraded crystal for each of the thermal histories. Symbols are as for Fig. 1, with red for one bad neighbor and black symbols for multiple bad neighbors. For comparison, the 8 % analytical error zone is shown.

Figure 10: Quantifying the effect of abrasion on isolated crystals for thermal histories featuring reheating. (A) The set of 100 Ma thermal histories used in the model. Peak burial occurs at 50 Ma with peak temperature from 10 to 80 °C. (B) The predicted age for spherical apatite grains of radius of 60 μm and different degrees of abrasion as a function of peak reheating temperature. He age for the non-abraded grain uses F_T correction, and two abraded grains (20 and 25 μm removed) are non-corrected. (C) The difference in age between 0 μm abrasion and 20 μm abrasion as a function of peak reheating temperature and crystal size (60, 80 and 100 μm). (D) The difference in age between 20 μm abrasion and 25 μm abrasion as a function of peak reheating temperature and crystal size (60, 80 and 100 μm). All models incorporate simultaneous ejection and diffusion for homogeneous crystals using Farley (2000) diffusion kinetics.

Figure_1

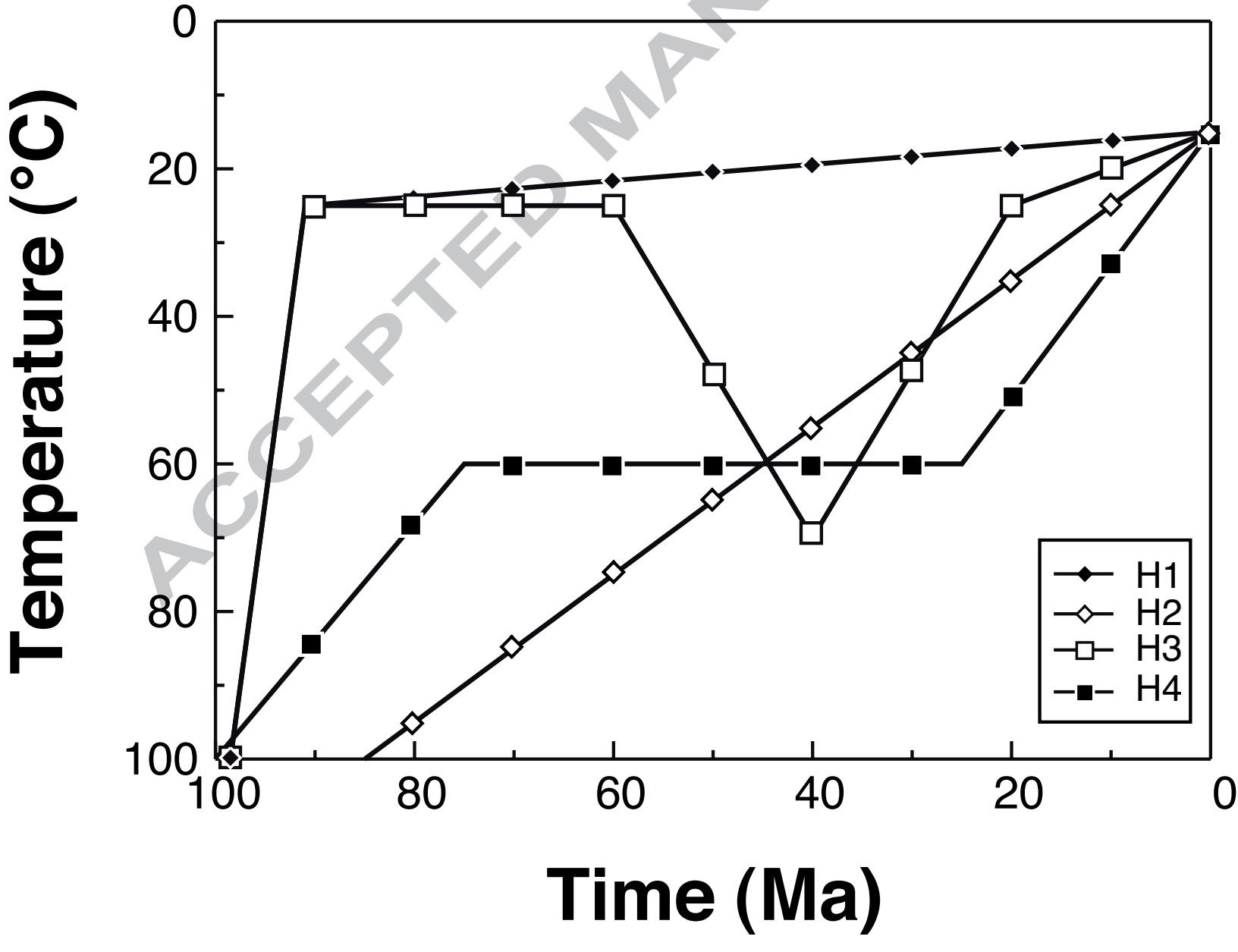

Figure_2

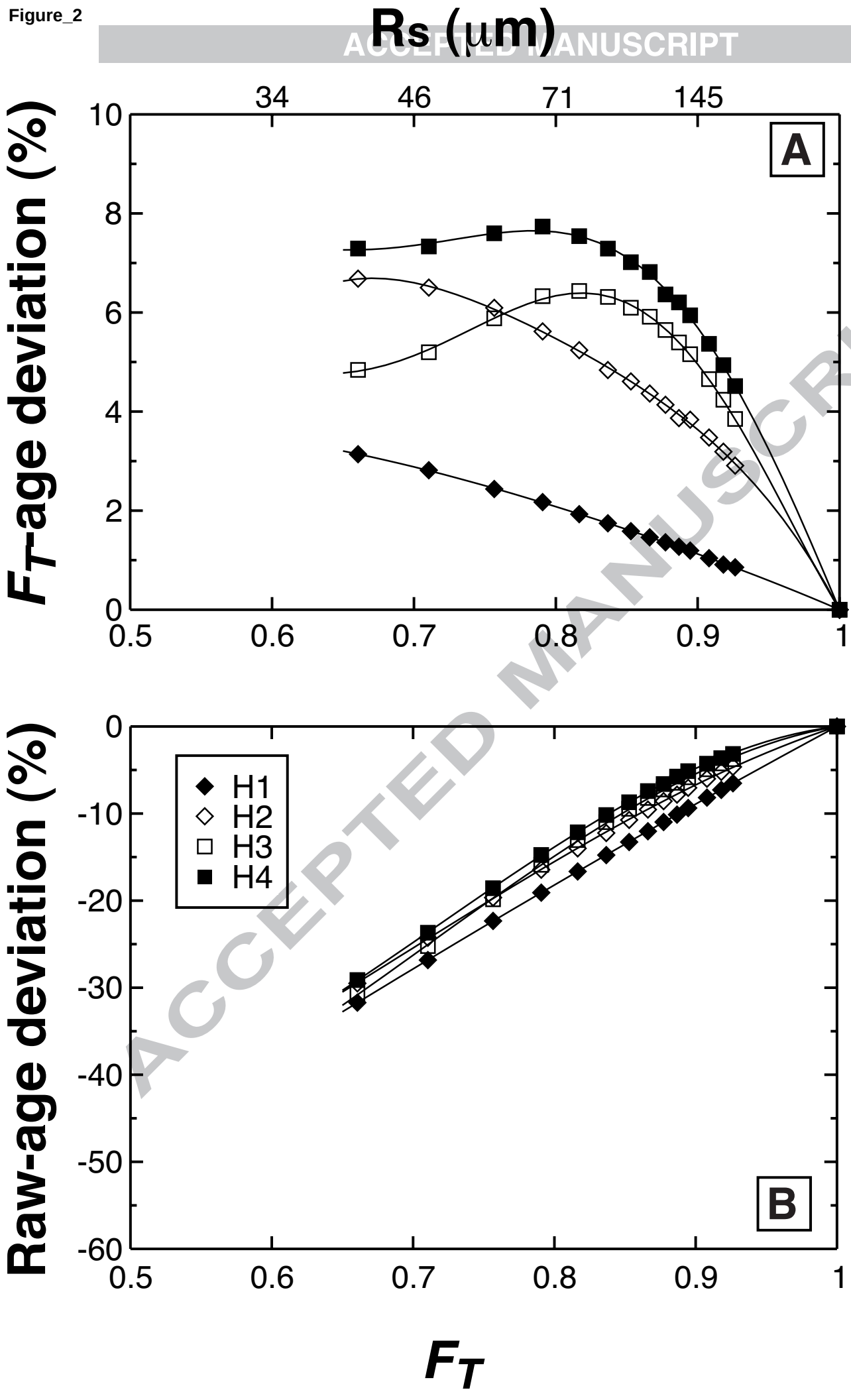

Figure_3

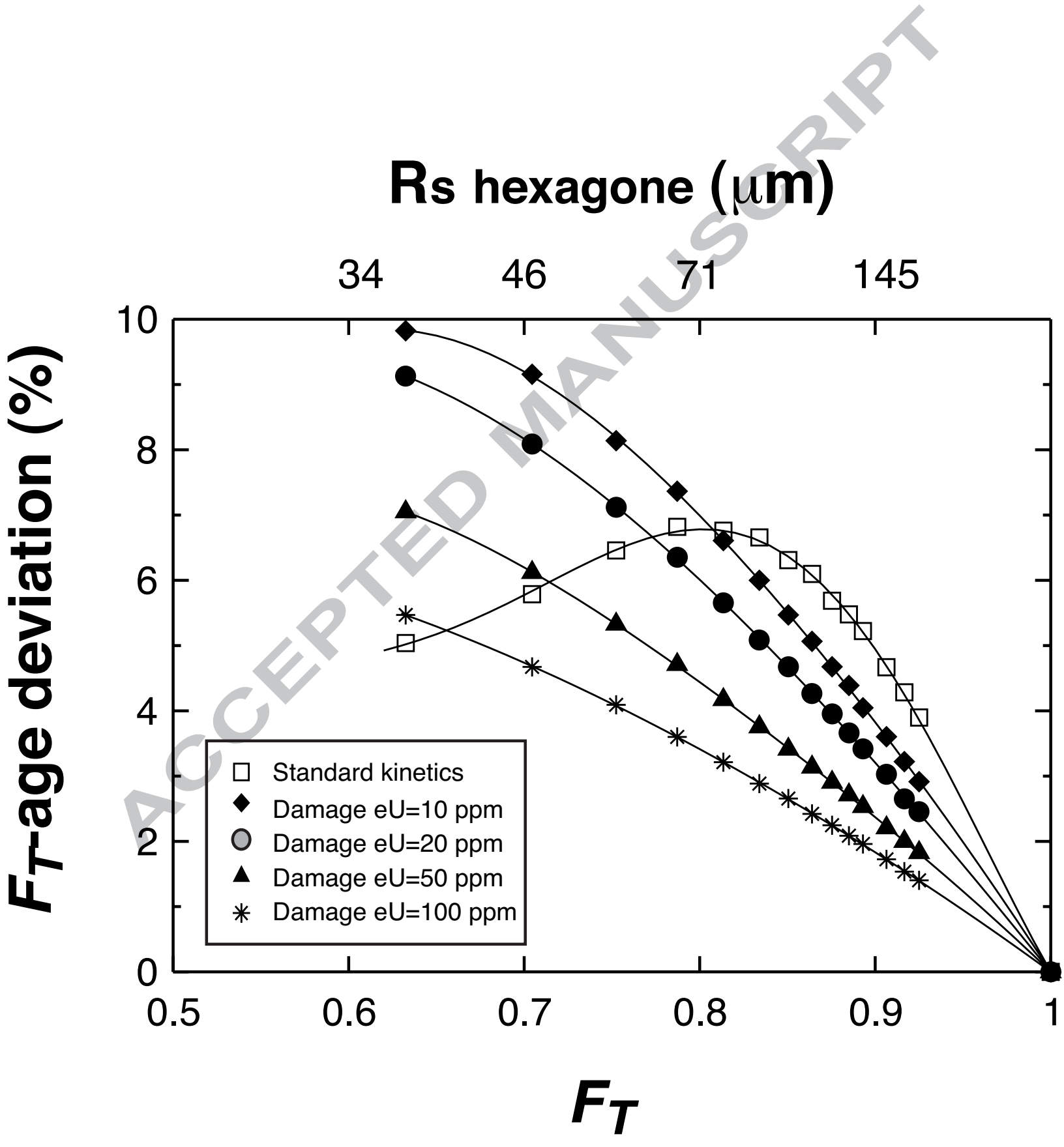

Figure_4

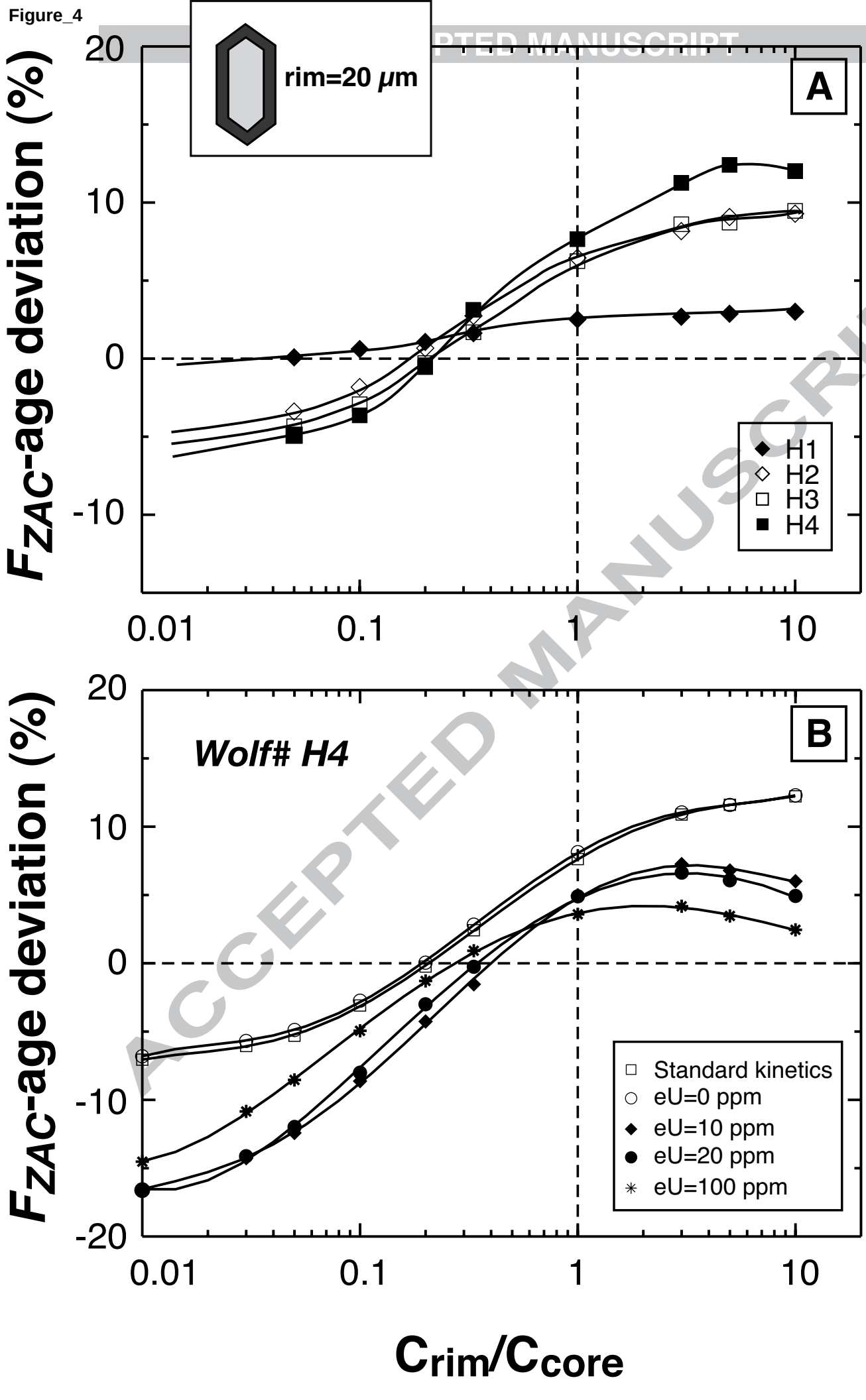

Figure_5

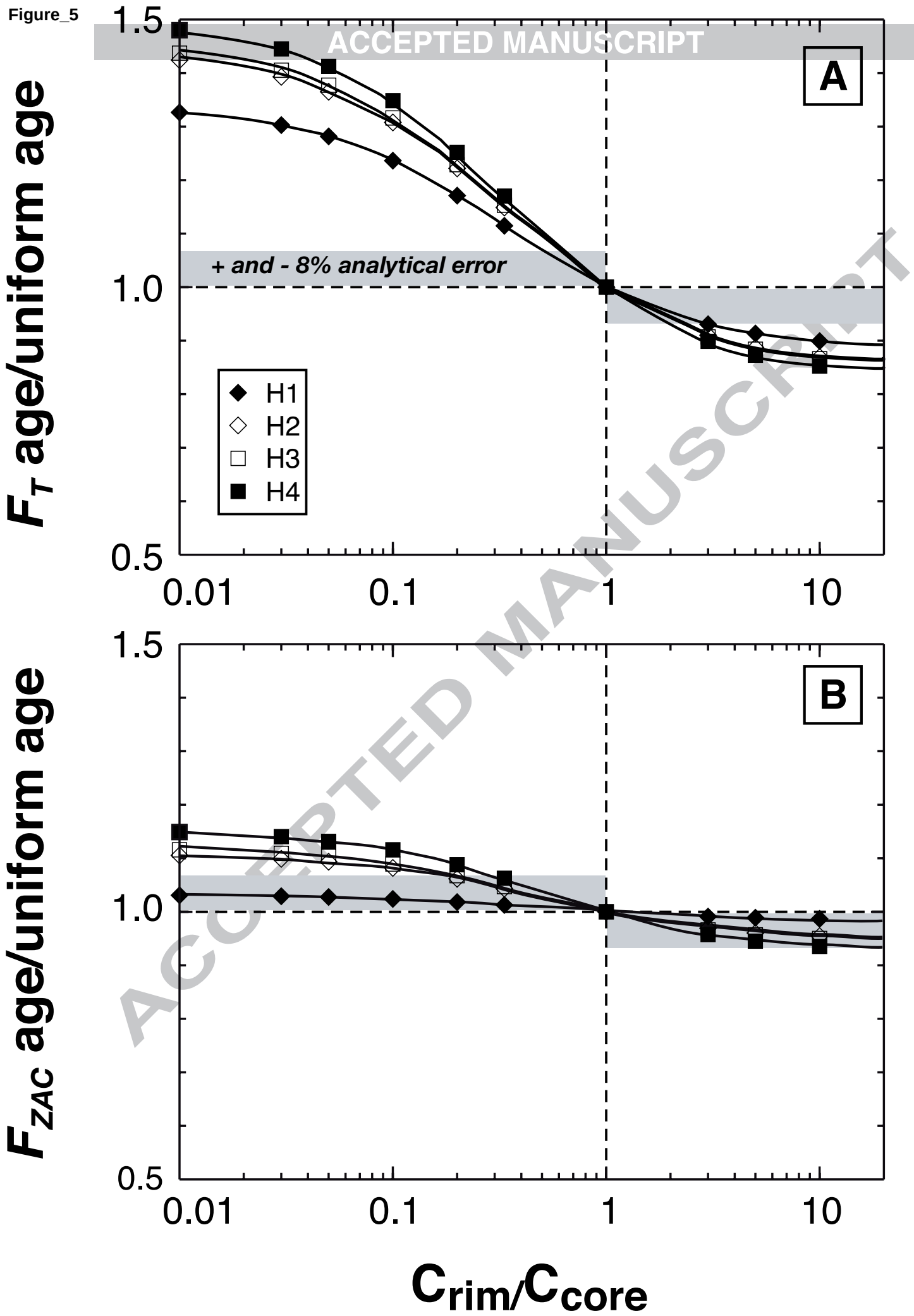

Figure_6

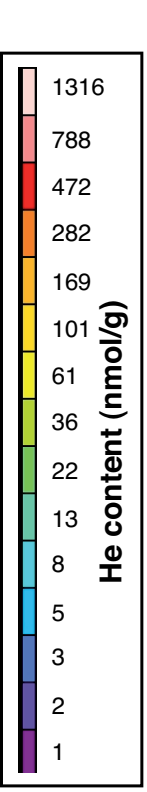

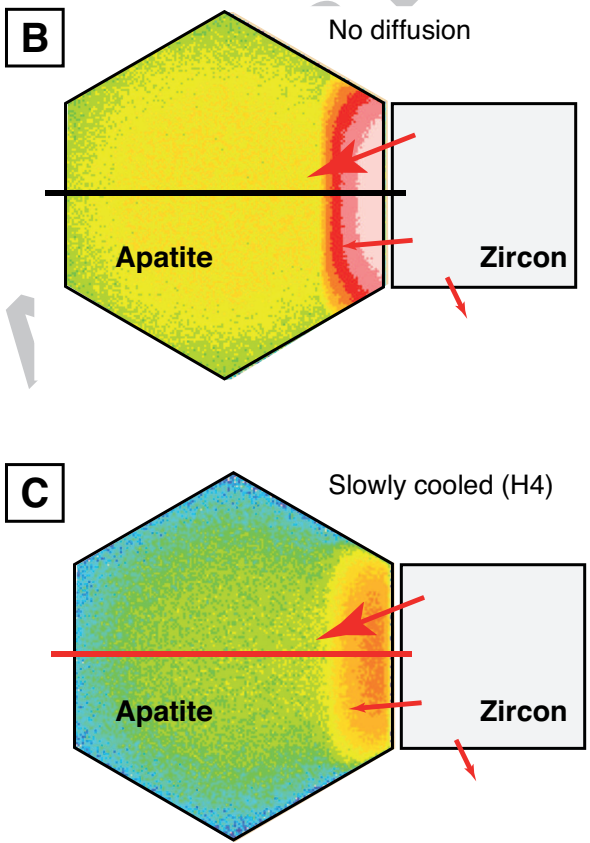

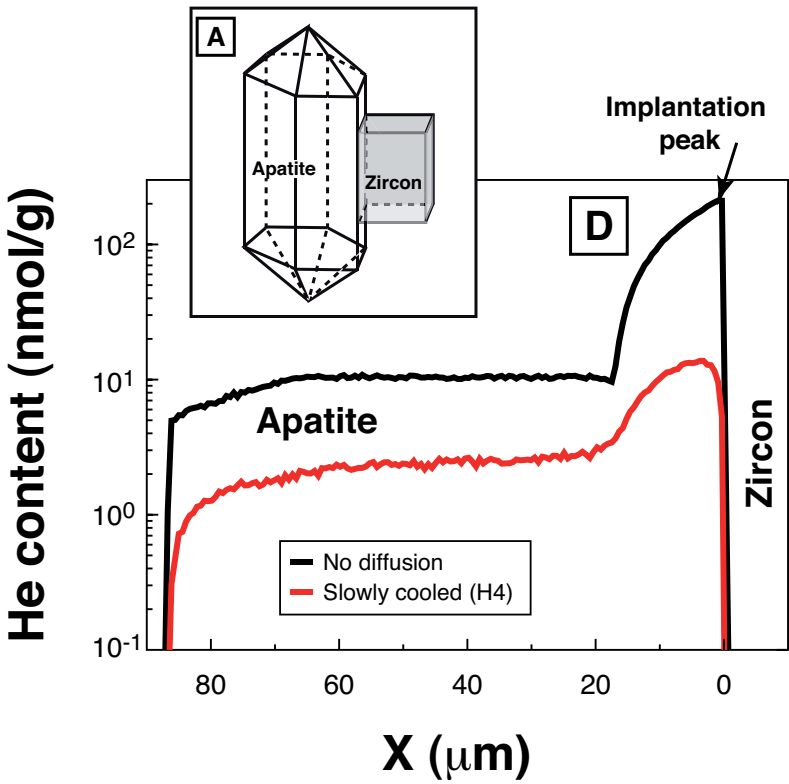

Figure_7

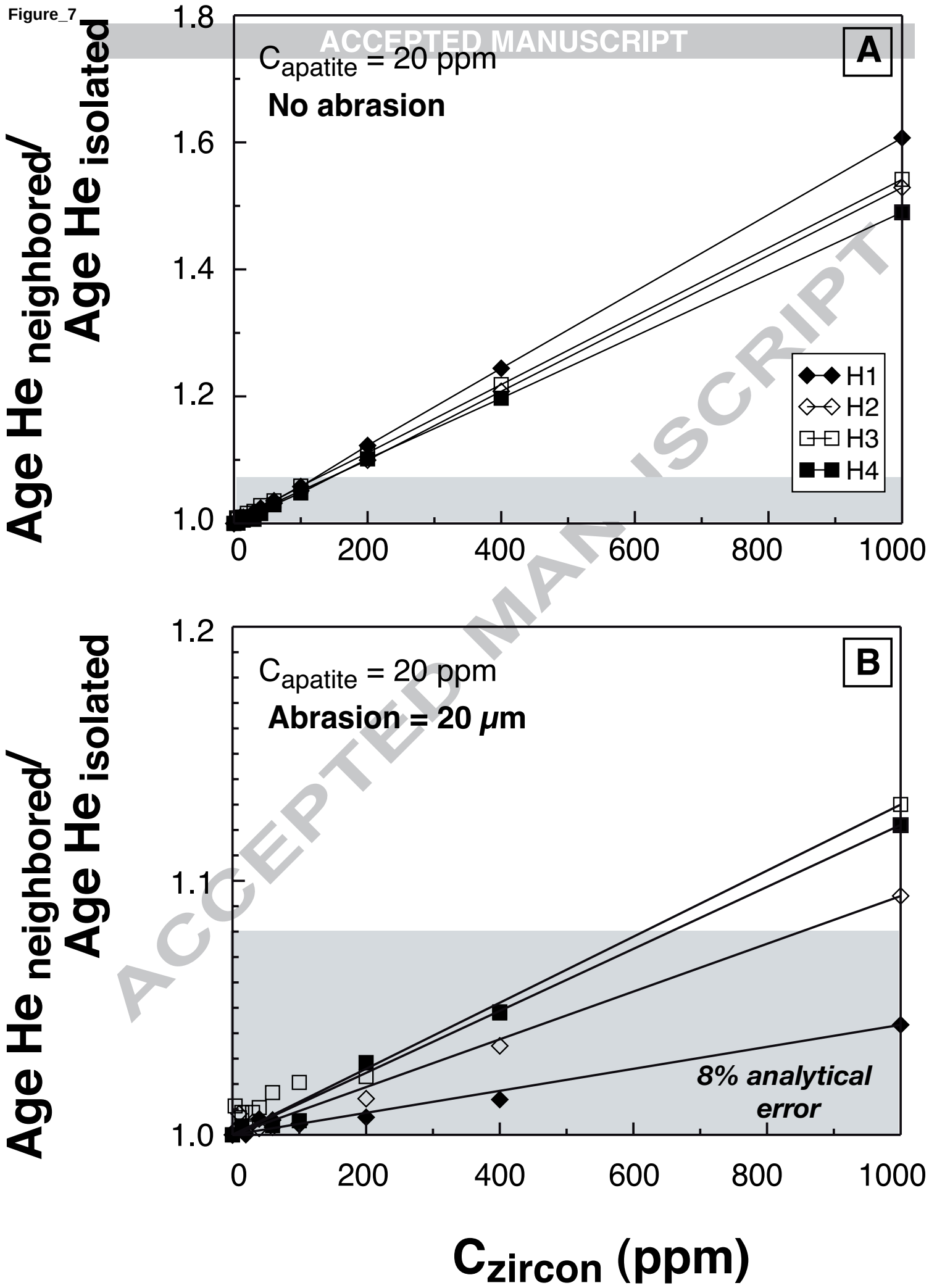

Figure_8

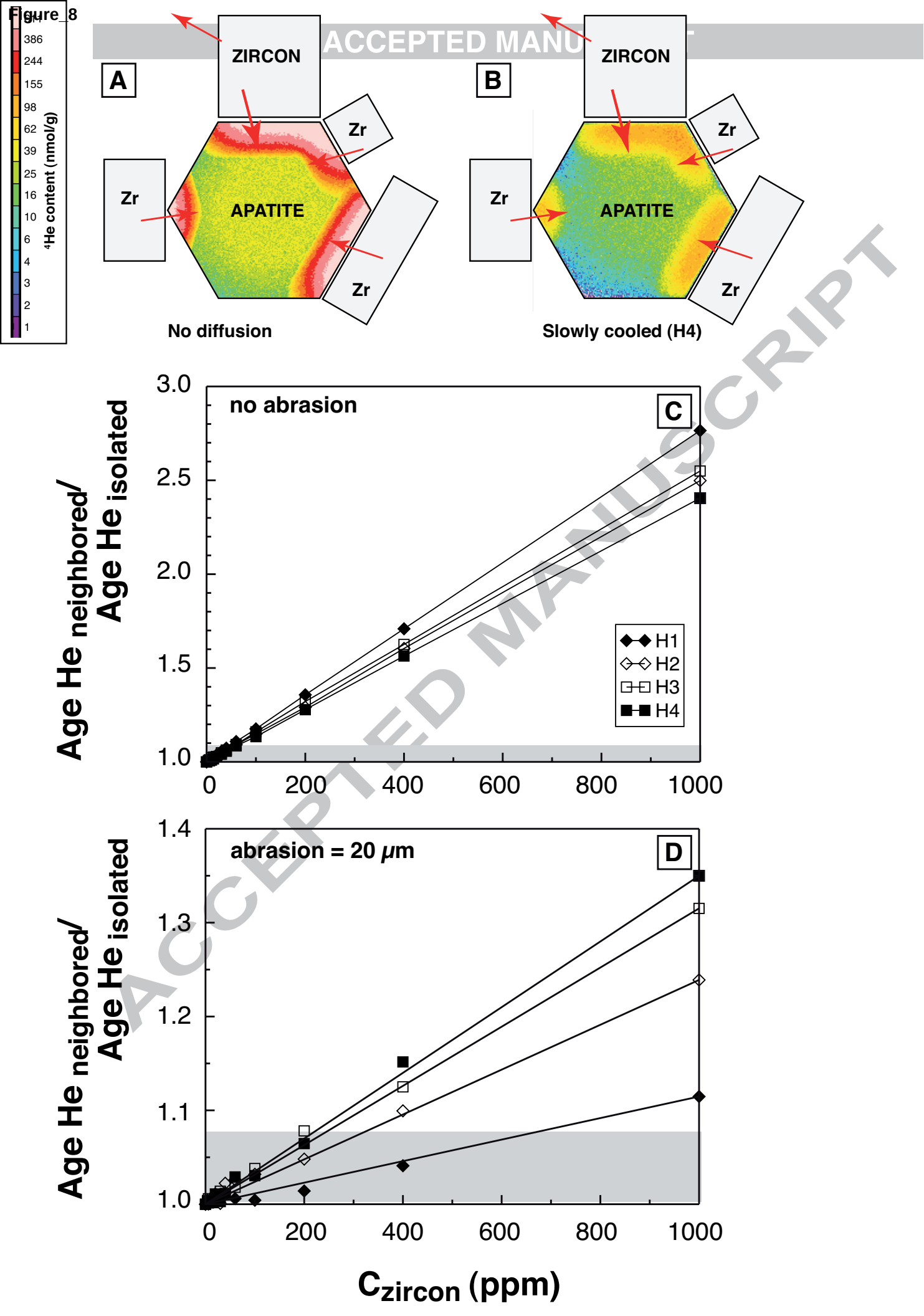

Figure_9

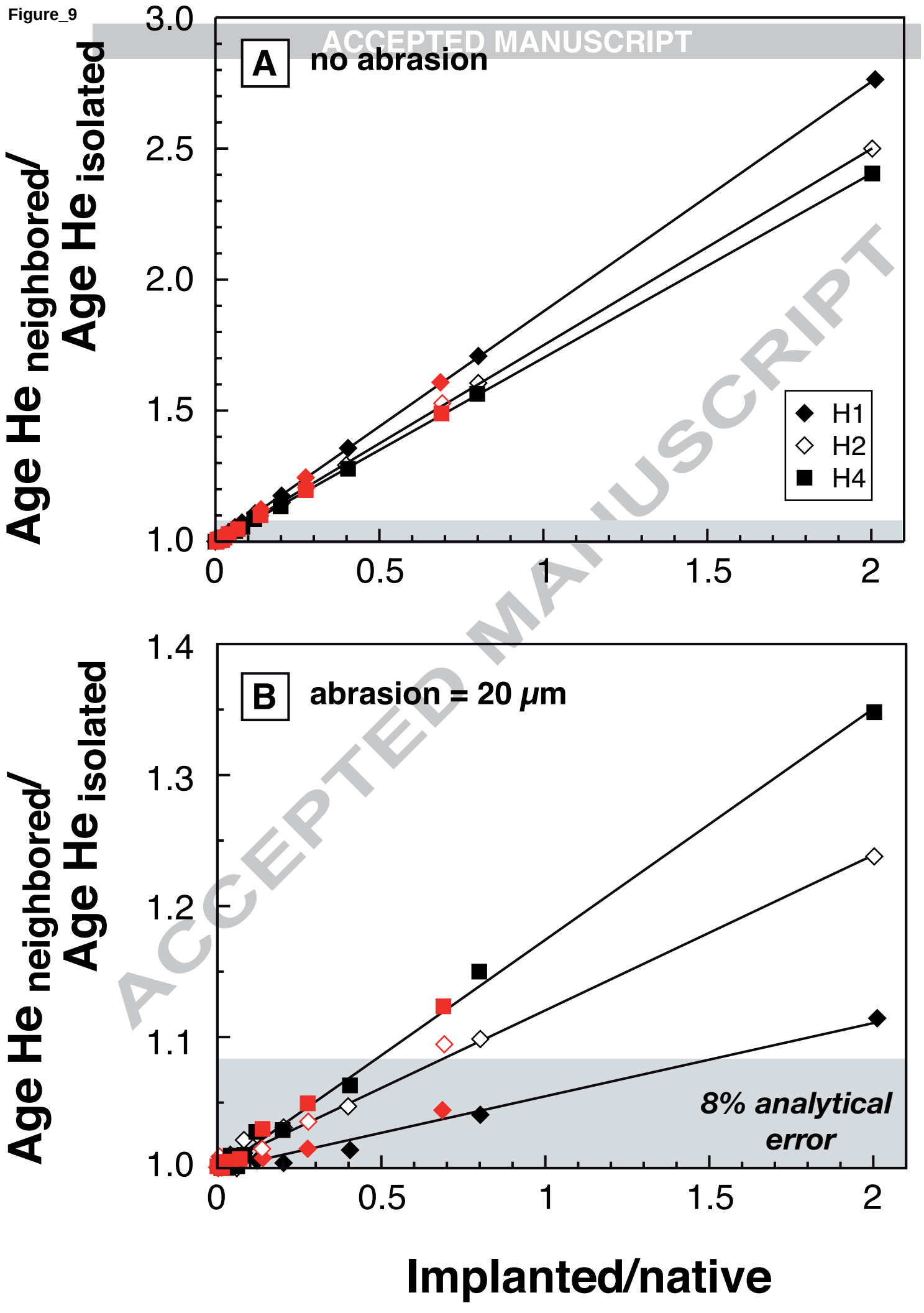

Figure_10